Chinese Chemical Letters 33 (2022) 2919–2922

Contents lists available at ScienceDirect

Chinese Chemical Letters

journal homepage: www.elsevier.com/locate/cclet

Valeriaquinone A, a unique anthraquinone–coumarin hybrid with selective inhibition of PTP1B from *Knoxia valerianoides*

Yan Jiang[1], Ren-Yong Yang[1], Zhao-Xia Qu, Gui-Ge Hou, Wei Cong, Chun-Hua Wang, Feng Zhao*

The Key Laboratory of Prescription Effect and Clinical Evaluation of State Administration of Traditional Chinese Medicine, School of Pharmacy, Binzhou Medical University, Yantai 264003, China

ARTICLE INFO

Article history:
Received 5 September 2021
Revised 12 October 2021
Accepted 25 October 2021
Available online 30 October 2021

Keywords:
Knoxia valerianoides
Anthraquinone–coumarin hybrid
PTP1B inhibitory activity
Cytotoxic activity
Allosteric inhibition

ABSTRACT

Valeriaquinone A (**1**), an unprecedented anthraquinone–coumarin hybrid, was isolated from the roots of *Knoxia valerianoides*. Its structure was determined by extensive spectroscopic analyses and X-ray diffraction. The plausible biosynthetic pathways for **1** were proposed. Compound **1** exhibited strong protein tyrosine phosphatase 1B (PTP1B) inhibition with high selectivity (> 30 fold) over homologous T cell protein tyrosine phosphatase (TCPTP) potentially by binding to an allosteric site predicted by kinetic analysis and molecular docking. Moreover, compound **1** showed significant cytotoxic activities against three human hepatoma cell lines (HepG2, QGY-7703, and SMMC-7721) with half maximal inhibitory concentration (IC_{50}) values of 1.39 ± 0.2, 10.34 ± 2.09, and 5.56 ± 0.47 μmol/L, respectively.

Natural anthraquinones comprise an important class of secondary metabolites with a 9,10-anthracenedione core derived from polyketides or chorismate/*o*-succinylbenzoic acid [1,2], and show a range of biological activities such as anticancer, laxative, anti-inflammatory, antibacterial, and hypoglycemic activities [3–5]. Their structural diversity mainly originates from biological oxidation and glycosylation of the benzene rings, and homodimerization of monomeric subunits [3]. Fewer anthraquinone derivatives are characterized by anthraquinone–xanthone heterodimers [6–8], and anthraquinone-based antibiotics [9–13]. Natural coumarins are a large group of heterocyclic compounds exhibiting versatile bioactivities, and most of them represent 7-hydroxycoumarin derivatives with various substitutions and conjugations, as well as regioisomeric dimers [14]. The benzo-α-pyrone motif of coumarin has also been demonstrated to be a unique pharmacophore in medicinal chemistry [15,16].

Knoxia valerianoides Thorel ex Pitard (Rubiaceae) is a perennial plant distributed in the southern regions of China. Its roots are used in traditional Chinese medicine as purgative and anti-ulcer agents. Our previous study on this plant led to the isolation of an array of *Rubia* type anthraquinones and pentacyclic triterpenoids, two lignans and a coumarin, and some of them showed antiviral, anti-inflammatory, and hepatoprotective activities [17–19]. As part of our continuous research, further investigation on *K. valerianoides* resulted in the identification of an unprecedented anthraquinone–coumarin hybrid, valeriaquinone A **(1)** (Fig. 1). Herein, we describe the isolation, structure elucidation, proposed biosynthetic pathways, and bioassay of **1**.

Valeriaquinone A **(1)** was initially obtained as an orange-yellow solid, and its molecular formula was determined as $C_{25}H_{16}O_9$ by high resolution electrospray ionization mass spectroscopy (HRESIMS) ion at *m/z* 459.0710 $[M–H]^-$ (calcd. for 459.0722) combined with ^1H and ^{13}C nuclear magnetic resonance (NMR) spectroscopic data (Table 1), accounting for 18 degrees of unsaturation. Compound **1** showed UV/vis absorption maxima (CH_3OH) at 204, 239, 281, 336, and 407 nm that were similar to those for previously obtained hydroxyanthraquinones [17,18]. The infrared spectroscopy (IR) spectrum displayed absorption bands for hydroxyl (3743 and 3304 cm^{-1}), conjugated carbonyl (1663 cm^{-1}), and aromatic ring (1590 and 1512 cm^{-1}) groups. The ^{13}C NMR, distortionless enhancement by polarization transfer (DEPT), and ^1H-detected heteronuclear single quantum coherence spectroscopy (HSQC) spectra showed a total of 25 carbon signals assignable to two carbonyls at δ_C 186.8 and 182.4 typical for an anthraquinone scaffold, 21 sp^2-hybridized carbons (ranging from δ_C 100.3 to 163.9) including 7 methines and 14 nonprotonated carbons, a methoxyl (δ_C 56.3), and an aliphatic methylene group (δ_C 23.4). The ^1H NMR spectrum showed resonances for four downfield shifted aromatic protons [δ_H 7.93 (ddd, J = 7.0, 7.0, 1.75 Hz), 7.95 (ddd, J = 7.0, 7.0, 1.95 Hz), 8.19 (dd, J = 7.0, 1.75 Hz), and 8.24 (dd, J = 7.0, 1.95 Hz)] attributable

* Corresponding author.
E-mail address: zhaofeng2015@163.com (F. Zhao).
[1] These authors contributed equally to this work.

https://doi.org/10.1016/j.cclet.2021.10.072
1001-8417/

Table 1
^{1}H (500 MHz) and ^{13}C (125 MHz) NMR Data for **1** in DMSO-d_6 (δ in ppm, J in Hz).

No.	δ_H (J in Hz)	δ_C (DEPT[a])	No.	δ_H (J in Hz)	δ_C (DEPT[a])
1		163.3, C	2′		161.8, C
2		117.7, C	3′		121.9, C
3		163.9, C	4′	7.18, t (1.5)[a]	139.0, CH
4	7.37, s	108.2, CH	5′	6.68, s	100.3, CH
4a		133.5, C	6′		145.8, C
5	8.19, dd (7.0, 1.75)	127.3, CH	7′		138.7, C
6	7.95, ddd (7.0, 7.0, 1.95)	135.2, CH	8′		133.1, C
7	7.93, ddd, (7.0, 7.0, 1.75)	135.1, CH	9′		138.4, C
8	8.24, dd (7.0, 1.95)	126.9, CH	10′		111.0, C
8a		133.3, C	1-OH	13.18, s	
9		186.8, C	3-OH	11.47, brs	
9a		109.8, C	6′-OCH_3	3.70, s	56.3, CH_3
10		182.4, C	7′-OH	9.36, brs	
10a		133.5, C	8′-OH	9.41, brs	
11	3.77, d (1.5)[a]	23.4, CH_2			

[a] Recorded at 600 MHz for ^{1}H NMR and 150 MHz for DEPT in DMSO-d_6.

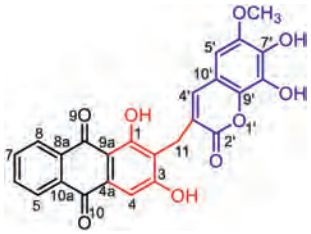

Fig. 1. Structure of compound **1**.

Fig. 2. Key ^{1}H–^{1}H COSY, HMBC, and NOESY correlations of **1**.

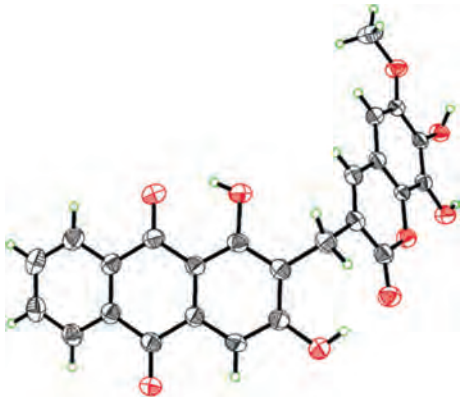

Fig. 3. X-ray Oak Ridge Thermal Ellipsoid Plot Program (ORTEP) drawing of **1**.

to an *ortho*-disubstituted benzene ring, a singlet aromatic proton (δ_H 7.37, s), and a hydrogen-bonded phenolic hydroxyl (δ_H 13.18, s). The aforementioned data indicated a 1,2,3-trisubstituted anthraquinone subunit for **1**, and that the hydroxyl (δ_H 13.18) was located at C-1. This fragment was corroborated by ^{1}H–^{1}H correlation spectroscopy (COSY) correlations of H-5/H-6/H-7/H-8, and heteronuclear multiple bond correlation spectroscopy (HMBC) correlations from H-4 (δ_H 7.37) to C-2 (δ_C 117.7), C-3 (δ_C 163.9), and C-10 (δ_C 182.4), from H-5 (δ_H 8.19) to C-10, from H-8 (δ_H 8.24) to C-9 (δ_C 186.8), and from 1-OH to C-1 (δ_C 163.3), C-2, and C-9a (δ_C 109.8) (Fig. 2). The hydroxyl (δ_H 11.47) was affixed to C-3 based on the downfield chemical shift of C-3 (δ_C 163.9) combined with nuclear overhauser effect spectroscopy (NOESY) correlations of OH-3/H-4. HMBC correlations of methylene protons (δ_H 3.77) with C-1, C-2, and C-3 confirmed the attachment of the methylene group to C-2.

Additionally, ^{1}H NMR spectrum showed $^4J_{H,H}$ couplings (J = 1.5 Hz) between H_2-11 and H-4′ (δ_H 7.18), indicating the presence of an allylic residue in **1** (Fig. 2 and Fig. S5 in Supporting information), which was in agreement with the observed ^{1}H–^{1}H COSY and NOESY cross-peaks of H_2-11/H-4′. The downfield shift of olefinic proton H-4′ (δ_H 7.18) suggested that a carbonyl group (C-2′) was connected to the double bond (C-3′=CH-4′). HMBC correlations from H_2-11 to C-2′ (δ_C 161.8), C-3′ (δ_C 121.9) and C-4′ (δ_C 139.0), and from H-4′ to C-11 (δ_C 23.4), C-2′, and C-3′ verified the linkages of CH_2-11–C-3′ and C-2′–C-3′=CH-4′. Considering the degrees of unsaturation, the proton signal at δ_H 6.68 (H-5′, s) was attributable to a pentasubstituted benzene ring, as evidenced by the HMBC correlations of H-5′/C-6′, C-7′, C-9′ and C-10′, OH-7′/C-6′, C-7′ and C-8′, and OH-8′/C-7′ and C-8′. The methoxy (δ_H 3.70) was placed at C-6′ based on the HMBC correlation of OCH_3/C-6′ and NOESY correlations of OCH_3/H-5′. The connection of C-4′–C-10′ was disclosed by HMBC correlations of H-4′/C-5′, C-9′, and C-10′, and NOESY correlations of H-4′/H-5′ (Fig. 2).

Apart from the above residues, an additional ring and an oxygen atom are required to satisfy the hydrogen deficiency and molecular formula, respectively. Thus, the carbonyl (C-2′) and C-9′ were proposed to be connected through an oxygen atom, forming a lactone ring, which was consistent with the quaternary carbon of C-9′ (δ_C 138.4) and the obvious upfield chemical shift of C-2′ (δ_C 161.8). The structure of **1** was further determined by X-ray diffraction analysis using Cu Kα radiation (Fig. 3, CCDC 1471733). Compound **1** is optically inactive and displayed no optical rotation values or Cotton effects.

The plausible biosynthetic pathways are proposed in Scheme 1. The biosynthetic precursors of **1** are traced to lucidin (**2**) and scopoletin (**3**). Lucidin is the major component from the title plant and shares the same substitution pattern as that of the anthraquinone moiety of **1**. Only a furanocoumarin, cnidilin, was obtained from *K. valerianoides* [19], thus the 7-hydoxrycoumarin derivative, scopoletin, was proposed to be another precursor. Briefly, dehydration of **2** could produce intermediate **i**. Then, a conjugate addition of **i** with **3** could yield **ii** [20], which undergoes further oxidation to afford **1** (Scheme 1A). Alternatively, the biosyn-

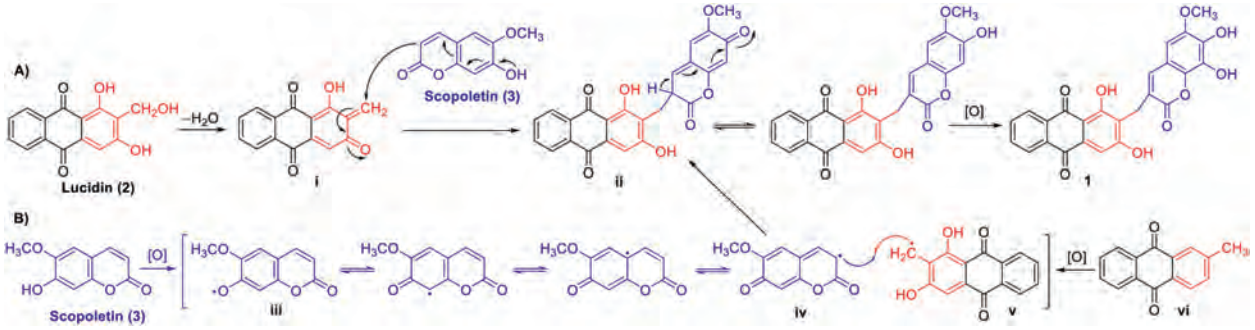

Scheme 1. Plausible biosynthetic pathways of **1**.

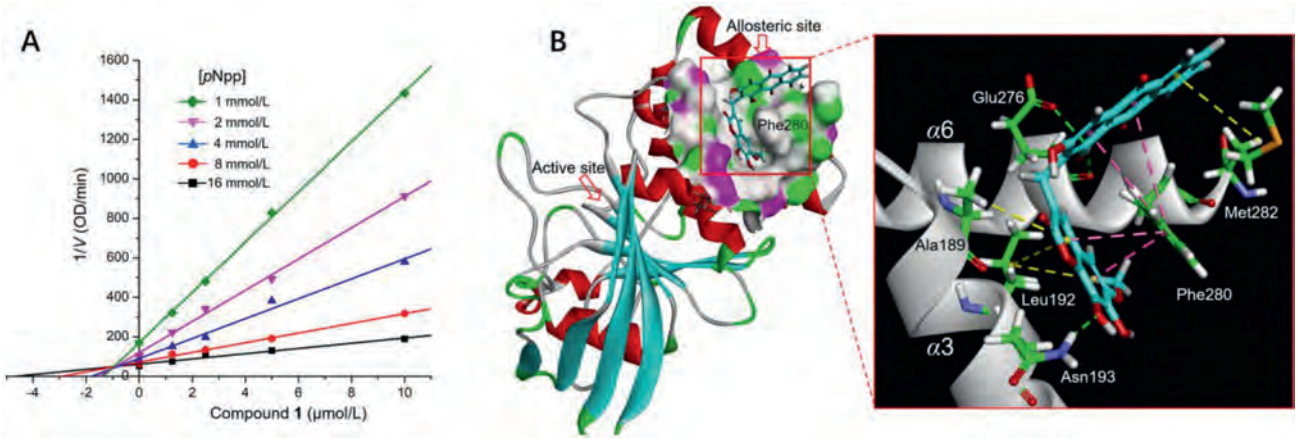

Fig. 4. (A) Dixon plot for PTP1B showing 1/*V versus* varying concentrations of **1** at *p*Npp concentrations of 1, 2, 4, 8, and 16 mmol/L. (B) 3D molecular docking model of compound **1** in the allosteric site of PTP1B (PDB code: 1T49). The key hydrogen bonds with Asn193 and Glu276, π-π stacks with Phe280, and π-alkyl interactions with Leu192, Ala189, and Met282 are shown with green, pink, and yellow dashed lines, respectively.

thesis might involve a free radical coupling reaction (Scheme 1B). Scopoletin (**3**) is still presumed to be a precursor. **3** undergoes initial oxidation through hydrogen atom abstraction from the 7′-OH to form a free radical intermediate **iii**. The free radical at 7′-O in **iii** migrates to C-3′ to produce radical **iv** [21], which suffers a radical coupling with the benzylic radical intermediate **v** generated in the oxidation process of anthraquinone precursor **vi** to form **ii**.

Furthermore, we attempted to perform the coupling reaction using **2** and **3** under reflux condition in methanol, or by reaction of the two subunits of **1**, fraxetin and co-isolated rubiadin, using $Cu(OAC)_2$ as a catalyst and *tert*–butylperoxy benzoate as the oxidant [22]. An additional strategy based on the formation of the methylene bridge in dicoumarol [23] was also developed by reaction of fraxetin and co-isolated xanthopurpuin with formaldehyde under mild conditions. All the above attempts turned out to be fruitless providing partial evidences for the natural occurrence of **1**.

The protein tyrosine phosphatase (PTP) 1B negatively regulates insulin signaling pathway through dephosphorylation of the insulin receptor and is highly validated as a therapeutic target for type 2 diabetes [24]. Moreover, PTP1B is also implicated in a variety of disorders, including cancer [25], inflammation [26], and cardiovascular diseases [27]. However, due to the charged catalytic site that is conserved among all PTPs, the designed phosphotyrosine mimetics suffer from poor selectivity and bioavailability, and none of them has as yet successfully passed the clinical trials. The hydrophobic and less conserved allosteric sites are demonstrated to be unique alternative targets for developing selective and cell-permeable PTP1B inhibitors [28,29]. *In vitro* bioassays revealed that compound **1** showed significant inhibitory effect on PTP1B activity with an half maximal inhibitory concentration (IC_{50}) value of 2.42 μmol/L. Notably, compound **1** exhibited 30.3-fold selectivity for PTP1B over the homologous phosphatase T cell protein tyrosine phosphatase (TCPTP) which shares 75% sequence identity with PTP1B in the catalytic domain (Table S1 in Supporting information). Further kinetic analysis and molecular docking were performed to elucidate the selective inhibition. Dixon-plot of the kinetic data showed intersecting lines in the *xy* region, revealing mixed-type inhibition of PTP1B with a K_i value of 0.96 μmol/L (Fig. 4 and Fig. S1 in Supporting information), which implied an allosteric mechanism of inhibition. Docking results indicated that compound **1** binds to the catalytic site and an allosteric site formed by helices α3 and α6. The latter complex conformation has lower binding energy and shows a binding mode similar to that of the reported benzofuran derivatives [28]. As shown in Fig. 4B, Compound **1** embeds the coumarin moiety in the hydrophobic pocket, and wraps around the central position Phe280 that is not conserved and replaced by cysteine in TCPTP. Strong π-π interactions between the rigid aromatic nucleus with Phe280, and hydrogen bonds with Asn193 and Glu276 were formed. Additional π-alkyl interactions with Leu192, Ala189 and Met282 were probably formed to enhance the binding potency of **1**. The docking results agreed with kinetic analysis and suggested the ability of **1** to block the interactions between helices α3-α6-α7 and trap PTP1B in the inactive conformation, which might account for its potency and selectivity for PTP1B (detailed *in silico* docking results were depicted in Figs. S2 and S3, and Table S2 in Supporting information.

Compound **1** was also evaluated for its cytotoxicity [30], and the results indicated that **1** exhibited cytotoxic activities against human hepatoma HepG2, QGY-7703 and SMMC-7721 cell lines

with IC_{50} values of 1.39 ± 0.2, 10.34 ± 2.09, and 5.56 ± 0.47 μmol/L, respectively, and had no significant effect on human lung adenocarcinoma A549 cells up to the concentration of 50 μmol/L (Table S3 in Supporting information).

In conclusion, valeriaquinone A **(1)**, a unique anthraquinone-coumarin hybrid, was isolated from the roots of *K. valerianoides*. The biosynthesis might involve a conjugate addition, or an alternative radical coupling reaction. Compound **1** showed selective PTP1B inhibition and was predicted to be an allosteric inhibitor based on kinetic analyses and molecular docking. Meanwhile, compound **1** showed significant cytotoxic activities. The characterization of **1** enriches the diversity of anthraquinone-, and coumarin-based dimers, and provides a template for development of novel selective PTP1B inhibitors.

Declaration of competing interest

The authors declare that they have no known competing financial interests or personal relationships that could have appeared to influence the work reported in this paper.

Acknowledgments

This work was financially supported by National Natural Science Foundation of China (No. 81703391), Shandong Provincial Natural Science Foundation of China (No. ZR2020KB015), and Key R&D Program of Shandong Province (No. 2019JZZY011104, China).

Supplementary materials

Supplementary material associated with this article can be found, in the online version, at doi:10.1016/j.cclet.2021.10.072.

References

[1] G. Bringmann, A. Irmer, D. Feineis, et al., Phytochemistry 70 (2009) 1776–1786.
[2] Y.S. Han, R. Van der Heijden, R. Verpoorte, Plant Cell Tissue Organ Cult. 67 (2001) 201–220.
[3] Y. Li, J.G. Jiang, Food Funct. 9 (2018) 6063–6080.
[4] É.S. Almeida, D. de Oliveira, D. Hotza, Compr. Rev. Food Sci. Food 18 (2019) 883–909.
[5] E.M. Malik, C.E. Müller, Med. Res. Rev. 36 (2016) 705–748.
[6] S.D. Holmbo, S.V. Pronin, J. Am. Chem. Soc. 140 (2018) 5065–5068.
[7] C. Tantapakul, T. Promgool, K. Kanokmedhakul, et al., Nat. Prod. Res. 34 (2020) 494–502.
[8] G.D. Anaya-Eugenio, D. Rebollar-Ramos, M. del Carmen González, et al., Chem. Biol. Interact. 311 (2019) 108798.
[9] J.W. Lown, Pharmacol. Ther. 60 (1993) 185–214.
[10] K.C. Nicolaou, Q. Cai, H. Sun, et al., J. Am. Chem. Soc. 138 (2016) 3118–3124.
[11] M.K. Kharel, P. Pahari, M.D. Shepherd, et al., Nat. Prod. Rep. 29 (2012) 264–325.
[12] Z. Wang, Z. Wen, L. Liu, et al., J. Nat. Prod. 82 (2019) 2483–2488.
[13] K.C. Nicolaou, D. Das, Y. Lu, et al., J. Am. Chem. Soc. 142 (2020) 2549–2561.
[14] H. Hussain, J. Hussain, A. Al-Harrasi, et al., Tetrahedron 68 (2012) 2553–2578.
[15] F.G. Medina, J.G. Marrero, M. Macías-Alonso, et al., Nat. Prod. Rep. 32 (2015) 1472–1507.
[16] I. Fotopoulos, D. Hadjipavlou-Litina, Med. Chem. 16 (2019) 272–306.
[17] F. Zhao, S. Zhao, J.T. Han, et al., Phytochem. Lett. 11 (2015) 57–60.
[18] F. Zhao, S. Wang, S. Lin, et al., Acta Pharm. Sin. B 2 (2012) 260–266.
[19] F. Zhao, S. Wang, X. Wu, et al., Chin. J. Chin. Mater. Med. 37 (2012) 2092–2099.
[20] W. Wang, X. Tang, F. Hua, et al., Org. Lett. 20 (2018) 2672–2675.
[21] B. Zhao, F.P. Guengerich, A. Bellamine, et al., J. Biol. Chem. 280 (2005) 11599–11607.
[22] S.L. Zhou, L.N. Guo, X.H. Duan, Eur. J. Org. Chem. 2014 (2014) 8094–8100.
[23] M.S. Spring, J.R. Stoker, Can. J. Biochem. 46 (1968) 1247–1251.
[24] Y. Tang, X. Zhang, Z. Chen, et al., Acta Pharm. Sin. B 8 (2018) 919–932.
[25] R.S. Banh, C. Iorio, R. Marcotte, et al., Nat. Cell Biol. 18 (2016) 803–813.
[26] L. Yang, Y.Y. Sun, Y.R. Liu, et al., Toxicol. Lett. 319 (2020) 11–21.
[27] P.A. Thiebaut, M. Besnier, E. Gomez, et al., J. Mol. Cell. Cardiol. 101 (2016) 50–57.
[28] C. Wiesmann, K.J. Barr, J. Kung, et al., Nat. Struct. Mol. Biol. 11 (2004) 730–737.
[29] N. Krishnan, D. Koveal, D.H. Miller, et al., Nat. Chem. Biol. 10 (2014) 558–566.
[30] Z. Qu, L. Ma, Q. Zhang, et al., Acta Crystallogr. C: Struct. Chem. 76 (2020) 269–275.